J|A|C|S ARTICLES

Published on Web 03/02/2009

Temperature- and Pressure-Induced Proton Transfer in the 1:1 Adduct Formed between Squaric Acid and 4,4′-Bipyridine

David M. S. Martins,[†] Derek S. Middlemiss,[‡] Colin R. Pulham,[†] Chick C. Wilson,[‡] Mark T. Weller,[§] Paul F. Henry,[||] Norman Shankland,[⊥] Kenneth Shankland,[#] William G. Marshall,[#] Richard M. Ibberson,[#] Kevin Knight,[#] Stephen Moggach,[†] Michela Brunelli,[▽] and Carole A. Morrison*[,†]

School of Chemistry and EaSTCHEM Research School, The University of Edinburgh, King's Buildings, West Mains Road, Edinburgh, EH9 3JJ, U.K., Department of Chemistry and WestCHEM Research School, University of Glasgow, University Avenue, Glasgow, G12 8QQ, U.K., School of Chemistry, University of Southampton, Highfield, Southampton, SO17 1BJ, U.K., Institut Laue-Langevin, BP156X, 38052 Grenoble, Cedex 9, France, Strathclyde Institute of Pharmacy and Biomedical Sciences, University of Strathclyde, Taylor Street, Glasgow, G4 ONR, U.K., ISIS Facility, STFC Rutherford Appleton Laboratory, Harwell Science and Innovation Campus, Chilton, Didcot, Oxon, OX11 0QX, U.K., and European Synchrotron Radiation Facility, BP 220-38043 Grenoble Cedex, France

Received October 28, 2008; E-mail: c.morrison@ed.ac.uk

Abstract: We have applied a combination of spectroscopic and diffraction methods to study the adduct formed between squaric acid and bypridine, which has been postulated to exhibit proton transfer associated with a single-crystal to single-crystal phase transition at ca. 450 K. A combination of X-ray single-crystal and very-high flux powder neutron diffraction data confirmed that a proton does transfer from the acid to the base in the high-temperature form. Powder X-ray diffraction measurements demonstrated that the transition was reversible but that a significant kinetic energy barrier must be overcome to revert to the original structure. Computational modeling is consistent with these results. Modeling also revealed that, while the proton transfer event would be strongly discouraged in the gas phase, it occurs in the solid state due to the increase in charge state of the molecular ions and their arrangement inside the lattice. The color change is attributed to a narrowing of the squaric acid to bipyridine charge-transfer energy gap. Finally, evidence for the possible existence of two further phases at high pressure is also presented.

1. Introduction

Proton-transfer plays a central role in many chemical and biological processes. From a fundamental perspective it is the mechanism by which nature achieves cell pH stabilization and can convert energy from one form into another.[1] From a technological perspective it underpins many of the current challenges in materials chemistry, including hydrogen storage and fuel cells.[2]

Within the field of molecular solid-state chemistry, there have been numerous studies on relatively simple model compounds, such as carboxylic acids, that exhibit proton-transfer across hydrogen bonds. The process is often associated with the adoption of alternative tautomeric forms and may be driven by an external stimulus such as light, temperature, or pressure.[3−12] The number of investigations characterized by diffraction techniques that have been reported is, however, quite low.[13−15] This can largely be attributed to experimental difficulties that are encountered when studying structure evolution of organic materials over a range of conditions. For example, accurate location of hydrogen atom positions at high temperatures or pressures using X-ray diffraction methods is difficult; single-crystal neutron diffraction studies are limited by crystal size; phase transitions associated with proton-transfer processes may be reconstructive resulting in loss of crystallinity or complete destruction of the crystal; and thermal decomposition processes

[†] The University of Edinburgh.
[‡] University of Glasgow.
[§] University of Southhampton.
[||] Institut Laue-Langevin.
[⊥] University of Strathclyde.
[#] STFC Rutherford Appleton Laboratory.
[▽] European Synchrotron Radiation Facility.

(1) Williams, R. J. P. *Annu. Rev. Biophys., Biophys. Chem.* **1988**, *17*, 71.
(2) Kreuer, K. D. *Chem. Mater.* **1996**, *8*, 610.
(3) Scherl, M.; Haarer, D.; Fischer, J.; DeCian, A.; Lehn, J.-M.; Eichen, Y. *J. Phys. Chem.* **1996**, *100*, 16175.
(4) Kümmer, L.; Wöhrl, H.; Haarer, D. *Chem. Phys. Lett.* **1994**, *227*, 337.
(5) Gilli, P.; Bertolasi, V.; Pretto, L.; Lycka, A.; Gilli, G. *J. Am. Chem. Soc.* **2002**, *124*, 13554.
(6) Desiraju, G. R.; Boese, R.; Jetti, R. K. R.; Thakur, T. S.; Vangala, V. R. *Chem. Commun.* **2004**, 2526.
(7) Brougham, D. F.; Horsewill, A. J.; Ikram, A.; Ibberson, R. M.; McDonald, P. J.; Pinter-Krainer, M. *J. Chem. Phys.* **1996**, *105*, 979.
(8) Middlemiss, D. S.; Facchini, M.; Morrison, C. A.; Wilson, C. C. *CrysEngComm* **2007**, *9*, 777.
(9) Wilson, C. C.; Goeta, A. E. *Angew. Chem, Int. Ed.* **2004**, *43*, 2095.
(10) Song, X.-J.; McDermott, A. E. *Magn. Reson. Chem.* **2001**, *39*, 37.
(11) Peng, B.-H.; Liu, G.-F.; Liu, L.; Jia, D.-Z. *Tetrahedron* **2005**, *61*, 5926.
(12) Chierotti, M. R.; Gobetto, R. *Chem. Commun.* **2008**, *14*, 1621.
(13) Wilson, C. C.; Shankland, N.; Florence, A. J. *Chem. Phys. Lett.* **1996**, *253*, 103.
(14) Wilson, C. C.; Xu, X.; Florence, A. J.; Shankland, N.; New, J. *Chem.* **2006**, *30*, 979.

 10.1021/ja8082973 CCC: $40.75

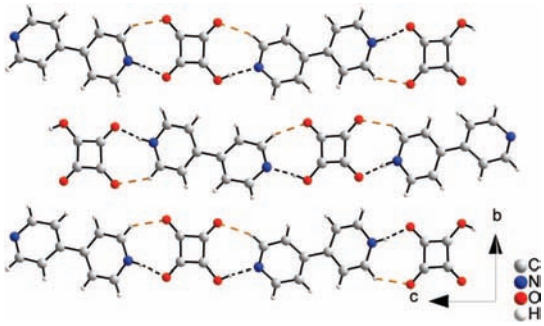

Figure 1. Crystal structure of SQBP form-I viewed along the *a* axis.

at elevated temperatures may limit the time-scales for data collection. Nevertheless, such studies are important if we are to improve our understanding of proton transfer processes in the molecular solid state.

One study that is of particular relevance in this area is that by Reetz et al.[15] (and highlighted by Bernstein[16]) in which temperature and pressure-induced phase transitions were observed in the 1:1 adduct formed between squaric acid and 4,4′-bipyridine (see Figure 1 for chemical structures). In this study, yellow (ochre), rectangular crystals of a monoclinic form-I were obtained from an aqueous solution of the two-component compounds, along with slightly darker crystals that were identified as a triclinic form. Differential scanning calorimetry (DSC) measurements showed that heating the yellow form-I to 453 K induced a first-order phase transition to a red polymorph (which we have chosen to label as form-II), with an energy uptake of 5.4 kJ mol^{-1}. On cooling to below 423 K, the color of the crystal changed back to yellow, but only 4.2 kJ mol^{-1} was released. Subsequent heating and cooling gave the red form at 446 K and the yellow form below 423 K, accompanied by an uptake and release of 4.2 kJ mol^{-1}. Further heating and cooling had no effect on the transition temperature or the magnitude of the energy changes. On the basis of this evidence and additional support from powder diffraction measurements, Reetz et al. suggested that the yellow form produced on cooling below 423 K was an additional polymorph. A partially deuterated sample prepared from squaric acid-d_2 and 4,4′-bipyridine was also studied. On heating to 453 K, no color change was observed and this apparent isotope effect led to the suggestion that the temperature-induced color change on heating form-I was due to proton transfer. Preliminary results of the response of the adduct to pressure were also obtained by applying a hydrostatic pressure of 11 kbar to a sample for 60 s. After decompression, X-ray powder diffraction and UV−visible data were collected and appeared similar to those obtained at high temperature, prompting Reetz et al. to suggest that the temperature-induced phase transition could also be induced via pressure.[15]

In the current study we have used a combination of spectroscopic and X-ray and neutron diffraction techniques to explore the effects of temperature and pressure on the crystal structures of the 1:1 adduct formed between squaric acid and 4,4′-bipyridine (subsequently denoted as SQBP). We have also applied a range of simulation techniques to complement the experimental studies to assess the energetics of the proton-transfer process and to identify the origin of the color change associated with the phase transitions.

2. Experimental Methods and Theoretical Basis

2.1. Materials. Squaric acid (SQ) and 4,4′-bipyridine (BP) were obtained from Sigma-Aldrich and used as received. Yellow rectangular crystals of form-I were grown by slowly cooling to 293 K (12 h) a hot aqueous solution (0.5 dm^3) containing squaric acid (0.44 g, 3.97 mmol) and 4,4′-bipyridine (0.62 g, 3.86 mmol). Single-crystal diffraction measurements confirmed the identity of these crystals as the monoclinic form-I of SQBP. Crystals of the perdeuterated adduct (SQBP-d_{10}) were prepared by slowly cooling to 293 K (12 h) a hot solution of squaric acid-d_2 (0.23 g, 1.98 mmol) and 4,4′-bipyridine-d_8 (0.32 g, 1.95 mmol) in D_2O (0.1 dm^3). Squaric acid-d_2 was obtained by repeated crystallization of squaric acid from D_2O; 4,4′-bipyridine-d_8 was obtained via exchange in the presence of $NaOD/D_2O$ under hydrothermal conditions as described by Browne et al.[17]

2.2. Optical and Infrared Studies. The infrared and visible spectra of the crystals were recorded with a Bruker Equinox-55 spectrometer linked to a Hyperion microscope attachment. Temperatures were controlled using a LINKAM LTS350 temperature stage (fitted with potassium bromide windows and purged with dry air) that was connected to a LNP94 cooling stage and controlled by a CI94 interface. The detectors used for the visible and infrared regions of the electromagnetic spectrum were a silicon diode and mercury cadmium telluride, respectively. Data were collected over the spectral ranges of 25000−8500 cm^{-1} (at a resolution of 8 cm^{-1}) and 6000−600 cm^{-1} (at a resolution of 2 cm^{-1}) within the temperature range 298−488 K (achieved with a heating and cooling rate of around 5 K/min). Corrections for background absorption were achieved by automatic subtraction of the spectrum of the empty temperature stage from the sample spectra.

2.3. Single-Crystal X-ray Diffraction. Variable-temperature diffraction data (180, 298, and 453 K) were collected on a single crystal of SQBP using a Bruker-SMART Apex CCD diffractometer [Mo Kα radiation (λ = 0.71073 Å)] equipped with an Oxford Cryosystems low-temperature device. Heating of the sample was controlled at around 6 K/min. The two lower temperature data collections corresponded to the form-I structure; the higher temperature to form-II. Data integration and reduction was performed using *SAINT* (Bruker Nonius).[18] An absorption correction was applied using the multiscan procedure program *SADABS*.[19] Structures were solved by direct methods using the *SIR92* package,[20] and refined against $|F|^2$ using all data.[21] Non-hydrogen atoms were refined with anisotropic thermal parameters. Hydrogen atoms associated with C−H bonds were placed in geometrically calculated positions. For form-I, at 180 and 298 K, H-atoms associated with N−H and O−H bonds were found on difference maps and subsequently restrained and refined. For form-II at 453 K the hydroxyl and amine H-atoms could not be located on a difference map and are therefore excluded from the high-temperature refinement. Crystal Data: Form-I, $C_{14}H_{10}N_2O_4$, 180 K, M = 270.24 g/mol, monoclinic, space group $P2_1/n$ with a = 3.7551(5) Å, b = 11.2066(13) Å, c = 27.322(3) Å; β = 92.947(7)°, Z = 4, V = 1148.2(2) $Å^3$, ρ_{calc} = 1.563 g/cm^3, R = 0.042 (R_w = 0.113) for 2996 independent reflections. The crystal selected was a yellow plate, 0.45 × 0.35 × 0.10 mm^3. Form-I, $C_{14}H_{10}N_2O_4$, 298 K,

(15) Reetz, M. T.; Hoger, S.; Harms, K. *Angew. Chem., Int. Ed. Engl.* **1994**, *33*, 181.
(16) Bernstein, J. *Polymorphism in Molecular Crystals, IUCr monographs on Crystallography*; Clarendon Press: Oxford, 2002.
(17) Browne, W. R.; O'Connor, C. M.; Killeen, J. S.; Guckian, A. L.; Burke, M.; James, P.; Burke, M.; Vos, J. G. *Inorg. Chem.* **2002**, *41*, 4245.
(18) *SAINT Area-Detector Software Package v7.01A*; Bruker AXS: Madison, WI, 2003.
(19) Sheldrick, G. M. *SADABS v2.04*; University of Göttigen: Göttingen, Germany, 2001.
(20) Altomare, A.; Cascarano, G.; Giacovazzo, C.; Guagliardi, A. *J. Appl. Crystallogr.* **1993**, *26*, 343.
(21) Watkin, D. J.; Prout, C. K.; Carruthers, J. R.; Betteridge, P. W.; Cooper, R. I. *CRYSTALS v12*; Chemical Crystallography Laboratory: Oxford, UK, 2003.

monoclinic, space group $P2_1/n$ with $a = 3.79750(10)$ Å, $b = 11.1996(3)$ Å, $c = 27.4424(7)$ Å, $\beta = 92.236(2)°$, $Z = 4$, $V = 1166.25(5)$ Å^3, $\rho_{calc} = 1.539$ g/cm^3, $R = 0.045$ ($R_w = 0.106$) for 2532 independent reflections. Form-II, $C_{14}H_{10}N_2O_4$, 453 K, monoclinic, space group $C2/c$ with $a = 12.359(8)$ Å, $b = 11.287(7)$ Å, $c = 9.061(6)$ Å; $\beta = 109.139(10)°$, $Z = 4$, $V = 1194.1(13)$ Å^3, $\rho_{calc} = 1.503$ g/cm^3; $R = 0.067$ ($R_w = 0.184$) for 851 independent reflections. The crystal was a red plate, $0.43 \times 0.22 \times 0.11$ mm^3.

2.4. Neutron Powder Diffraction. Variable-temperature diffraction data for SQBP-d_{10} were collected on the high-resolution powder diffractometer (HRPD) at the ISIS pulsed neutron source.[22] The lightly ground sample (~2 g) was placed in a 5 mm diameter cylindrical vanadium can and heated at a rate of 5 K per minute using a vanadium element furnace. Neutron time-of-flight spectra were recorded over a time-of-flight range between 30 and 130 ms. Diffraction data were recorded at 292 K for ca. 15 h. In order to investigate the temperature at which the phase transition was complete, data were recorded at 5 K intervals for ca. 10 min in the region 473−483 K. The remainder of time available for this experiment (ca. 10 h) was then used to collect data at 488 K. Data from gently ground crystals of the hydrogenous sample (SQBP, 0.75 g) were also collected on the D20 high-flux instrument at the Institut Laue Langevin ($\lambda = 1.869$ Å) in high-resolution mode[23] over the temperature range 120−473 K. The patterns were corrected for attenuation due to strong incoherent scattering from hydrogen and moderately strong preferred orientation along the (010) axis following the protocol given in International Tables C section 6.3.3 for a cylindrical can with $\mu R = 0.90$, calculated assuming 100% packing efficiency.[24] Data reduction was achieved using the standard data reduction protocols for the D20 instrument in LAMP.[23] Full-profile Rietveld[25] refinements of the resulting patterns were obtained using *PC-GSAS*[26] as implemented in the *EXPGUI* package.[27] Starting models used for both the low- and high-temperature structures were those obtained from the initial X-ray diffraction experiments. Geometrical restraints and thermal parameter constraints based on the X-ray structure were used in order to enhance the observable data to parameters ratio. Background parameters (shifted Chebyschev with 8 and 12 terms for forms-I and -II, respectively) and scale factor were also refined. The figures of merit obtained were $R(F^2) = 0.1060$ and $\chi^2 = 207.2$ for the low-temperature collection and $R(F^2) = 0.1413$ and $\chi^2 = 61.29$ for the high-temperature collection.

2.5. X-ray Powder Diffraction. Temperature-controlled experiments were performed on the high-resolution powder diffractometer of beam line (ID31) at the European Synchrotron Research Facility, Grenoble [$\lambda = 0.801003(3)$ Å].[29,30] SQBP form-I crystals (4 mg) were lightly ground and loaded into thin-walled borosilicate glass capillaries (diameter 1.5 mm), which were mounted on the axis of the diffractometer and spun rapidly to improve the powder averaging of the orientations of individual crystallites. The system was heated at a rate of 2 K/min from 293 to 493 K by means of an Oxford Cryosystems Cryostream device mounted coaxially to the capillary, and subsequently allowed to cool at a rate of ca. 10 K/min, for around 10 h, during which time four further data sets were collected at 420, 370, 320, and 270 K. Lattice parameters were obtained from Pawley refinements[28] in the 2θ range 2−40° using the programs *TOPAS*[29] and *DASH*.[30]

2.6. Plane-Wave Basis Set Modeling. Density functional theory (DFT) calculations were performed using the CPMD package.[31] Initial geometries, unit cells, and space group symmetry constraints for SQBP forms-I and -II were taken from the X-ray diffraction results with the hydrogen atoms placed manually on the bipyridine molecule in the case of the high-temperature form. Electronic exchange and correlation were incorporated within the gradient-corrected functional of Perdew, Burke, and Ernzerhof (PBE).[32,33] Core electrons were treated using a set of Vanderbilt ultrasoft pseudopotentials,[34] while valence electrons were represented by a plane-wave basis set truncated at an extended energy cutoff of 30 Ry. In CPMD the maximum energy gradient component controls the optimization process, which was set at 5×10^{-4} au. The energy tolerance, controlling the self-consistent field (SCF) convergence, was set at 10^{-5} au. In view of the poor representation of weak interactions within standard DFT approaches, no attempt was made to optimize the cell volume or lattice vectors. It should be noted that the a axis of the form-I structure is considerably shorter than the other two; as CPMD does not support the use of multiple k-points to sample the electronic band structure the present simulations used a $3 \times 1 \times 1$ supercell to create a model of more cubic dimensions. Following optimization, potential energy surface (PES) scans were undertaken to mimic the form-I to form-II (and reverse) phase transition. In the first case energies were obtained in the form-I structure while a proton was pulled in set increments along an N···O hydrogen bond from a squaric molecule to bipyridine; in the second case, calculations were applied to the form-II structure while a proton was shifted from a bipyridine molecule back to a squaric. Finally, NVT-ensemble molecular dynamics (MD) simulations were carried out at target temperatures of 180 K for form-I and 350 K for form-II. A time step of 3.0 au was used, while each degree of freedom was coupled to a chain of four Nosé−Hoover thermostats[35,36] at a characteristic frequency of 3000 cm^{-1}. An electronic mass parameter of 400 au was employed.

2.7. Localized Basis Set Modeling. Solid state calculations using the CRYSTAL06 code[37] were applied to both forms of SQBP. Standard 6-311G** basis sets were employed,[38,39] while exchange and correlation were included by use of the B3LYP hybrid functional.[40−42] We note that this method has previously been shown to give band dispersions and gap widths in good agreement with experiment for a wide range of materials.[43,44] As with the plane-wave simulations, no attempt was made to optimize the cell parameters. Atom optimizations employed a total energy convergence tolerance of 10^{-7} au and were pursued until rms gradients and displacements fell below 3×10^{-4} and 1.2×10^{-3} au, with tolerances for the maximum component and maximum absolute value respectively of 1.5 times the rms setting. Electronic band structures were sampled using a $4 \times 4 \times 4$ Monkhorst−Pack

(22) Ibberson, R. M.; David, W. I. F., Knight, K. S. *Report RAL-92-031*; Rutherford Appleton Laboratory: Chilton, UK, 1992.
(23) Hansen, T. C.; Henry, P. F.; Fischer, H. E.; Torregrossa, J.; Convert, P. *Meas. Sci. Technol.* **2008**, *19*, 034001.
(24) Maslen, E. N. *Int. Tables Crystallogr.* **2006**, *6*, 600.
(25) Rietveld, H. M. *Acta Crystallogr.* **1967**, *22*, 151.
(26) Larson, A. C.; Von Dreele, R. B. *GSAS, Report LAUR86-748*; Los Alamos National Laboratory: Los Alamos, NM, 2004.
(27) Toby, B. H. *J. Appl. Crystallogr.* **2001**, *34*, 210.
(28) Pawley, G. S. *J. Appl. Crystallogr.* **1981**, *14*, 357.
(29) Coelho, A. A. *TOPAS*; Bruker AXS: Karlsruhe, Germany, 2003.
(30) David, W. I. F.; Shankland, K.; van de Streek, J.; Pidcock, E.; Motherwell, W. D. S.; Cole, J. C. *J. Appl. Crystallogr.* **2006**, *39*, 910.
(31) *CPMD version 3.11.1, Copyright IBM Corp.* 1990−2006, Copyright MPI für estkörperforschung Stuttgart, 1997−2001.
(32) Perdew, J. P.; Burke, K.; Ernzerhof, M. *Phys. Rev. Lett.* **1997**, *78*, 1396.
(33) Perdew, J. P.; Burke, K.; Ernzerhof, M. *Phys. Rev. Lett.* **1996**, *77*, 3865.
(34) Vanderbilt, D. *Phys. Rev. B* **1990**, *41*, 7892.
(35) Nose, S. *J. Chem. Phys.* **1984**, *81*, 511.
(36) Hoover, W. G. *Phys. Rev. A* **1985**, *31*, 1695.
(37) Dovesi, R.; Saunders, V. R.; Roetti, C.; Orlando, R.; Zicovich-Wilson, C. M.; Pascale, F.; Civalleri, B.; Doll, K.; Harrison, N. M.; Bush, I. J.; D'Arco, P.; Llunell, M. *CRYSTAL06*; University of Torino: Torino, Italy, 2006.
(38) Krishnan, R.; Binkley, J. S.; Seeger, R.; Pople, J. A. *J. Chem. Phys.* **1980**, *72*, 650.
(39) McLean, A. D.; Chandler, G. S. *J. Chem. Phys.* **1980**, *72*, 5639.
(40) Becke, A. D. *J. Chem. Phys.* **1993**, *98*, 5648.
(41) Lee, C.; Yang, W.; Parr, R. G. *Phys. Rev. B* **1988**, *37*, 785.
(42) Miehlich, B.; Savin, A.; Stoll, H.; Preuss, H. *Chem. Phys. Lett.* **1989**, *157*, 200.
(43) Muscat, J.; Wander, A.; Harrison, N. M. *Chem. Phys. Lett.* **2001**, *342*, 397.
(44) Perger, W. F. *Chem. Phys. Lett.* **2002**, *368*, 319.

mesh[45] and subsequently visualized via atom-projected densities-of-states plots; charge distributions were obtained from Mulliken analyses. Finally, isolated molecule calculations were undertaken using the *Gaussian03* suite of programs,[47] adopting the same B3LYP Hamiltonian as used in the periodic simulations, but employing larger 6-311++G** basis sets so as to provide the diffuse functions necessary for the proper description of the anionic states of the squaric molecule. We note that such extensive basis sets are generally not required in solid-state calculations, as functions at neighboring sites assist in the representation of diffuse electronic states. Harmonic vibrational analyses were performed subsequent to the optimizations.

3. Results and Discussion

3.1. Optical and Infrared Studies. On heating a single crystal of form-I to ca. 453 K the crystal turned red with no apparent disintegration. This red form was presumed to be form-II. Visible spectroscopic measurements showed an absorption band centered at 450 nm at ambient temperatures for form-I, with a new absorption band appearing on heating above 453 K centered at 540 nm that is consistent with the observed color change. Variable-temperature infrared spectra were also collected on a crystal in order to characterize the phase transition. Direct comparison of the spectra recorded at low and high temperatures was only possible in the region 2000−4000 cm^{-1} on account of the strong absorption of the form-II crystal in the region below 2000 cm^{-1} combined with the increased scattering from the sample, presumably as a consequence of degraded crystal quality. A difference between the two spectra was observed, with the appearance of a new band at 3050 cm^{-1} in form-II. This region of the spectrum corresponds to aromatic C−H stretching modes and hydrogen bonded N−H modes. Hence, the appearance of this band at high temperature suggests either changes in the aromatic rings of the bipyridinium ions or changes associated with migration of a proton toward a nitrogen atom of a bipyridinium ion. The optical and infrared spectra recorded are available in the Supporting Information.

3.2. Single-Crystal X-ray Diffraction Studies. At room temperature, SQBP form-I crystallizes in space group $P2_1/n$ with both the acid and base present in their monoprotonated forms [Figure 1]. The bipyridinium cation is twisted, with a torsion angle between the heterocyclic rings of 23.9(2)° and connects to the squaric acid anion primarily through N−H···O [N···O = 2.6058(18) Å] and O−H···N [O···N = 2.6291(18) Å] hydrogen bonds to form $C_2^2(14)$ chains which lie parallel to the (103) plane. Two auxiliary C−H···O hydrogen bonds are also formed within the chain [C···O = 3.214(2) and 3.125(2) Å]. Interacting between the planes are two C−H···O hydrogen bonds [C···O = 3.275(2) and 3.142(2)]. The latter C−H···O hydrogen bonds offset $\pi-\pi$ stacking interactions which also interact between the planes, with the shortest interaction between the centroids of the heterocyclic rings measuring 4.5531(9) Å.

In situ heating of a crystal of form-I to 453 K resulted in a single-crystal to single-crystal first-order phase transition to the high-temperature form-II, which adopted the monoclinic crystal system with space group *C*2/*c*. The observation that the crystal remains intact across this transition indicates that this phase transition is not destructive and that the crystal structures of the two forms are closely related. Note the protonation sites of the squaric acid and bipyridine molecules could not be reliably determined due to the high temperature employed in the data collection. In form-II the bipyridine molecules are now flat [with a torsion angle between the rings of just 1.3(6)°], but the pattern of intermolecular contacts observed in form-I is essentially maintained. The distance between the planes of the aromatic rings has decreased, with the shortest centroid-to-centroid distance between rings measuring 3.734(3) Å at 453 K. On undergoing the transition, the planes of molecules have also slipped by ca. 13° during the phase transition (Figure 2). Selected geometrical parameters for both polymorphs of SQBP are in Table 1 in the Supporting Information.

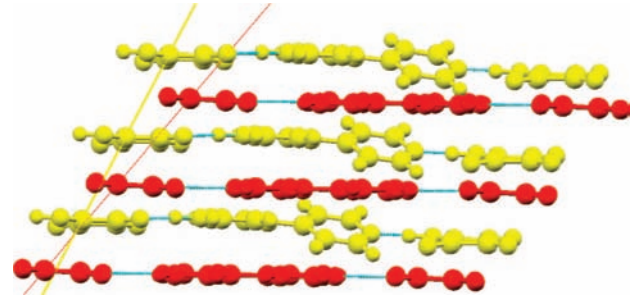

Figure 2. Comparison of form-I (yellow) and form-II (red) SQBP viewed along the *b* axis. The calculation of the slipping angle was based on the intercept of the yellow and red planes.

3.3. Neutron Powder Diffraction. These measurements were undertaken in order to locate the hydrogen atom positions in form-II. Ideally, single-crystal neutron diffraction would have been the technique of choice, but such studies require relatively large single crystals and, despite numerous attempts, it became clear that crystals of SQBP show a strong preference to grow as long but very thin plates that were not suitable for this type of experiment. Instead, it was decided to use neutron powder diffraction and initial experiments were performed using the high-resolution powder diffractometer (HRPD) located at the ISIS Neutron Facility, Rutherford Appleton Laboratory, UK. Note that a fully deuterated sample was used for these measurements as the strong incoherent neutron scattering cross section of hydrogen would superimpose a very high background signal on the resulting diffraction pattern.

Diffraction data collected at 292 K confirmed the presence of form-I, and this form persisted up until 488 K, at which point a new pattern was obtained which could be successfully indexed as form-II. This transition temperature is significantly higher than that observed for the nondeuterated compound, lending further support to the theory that the phase transition does involve proton transfer. (We note in passing that the temperature-dependent behavior of the partially deuterated compound in the study by Reetz et al. only explored as high as the original phase transition, and that in all likelihood this accounts for the absence of a phase transition for this isotopologue). Unfortunately, prolonged data collection for 12 h at this elevated temperature revealed the presence of new Bragg peaks that could not be attributed to either form-I or form-II, and which persisted on cooling the sample back to ambient temperature. This strongly suggested decomposition of the sample at high temperature, perhaps exacerbated by contact with the vanadium can. For this reason it was not possible to extract structural information from the form-II diffraction data, and it was therefore clear that more rapid data collection was required in order to prevent significant decomposition. An experiment was therefore conducted on the D20 diffractometer located at the

(45) Monkhorst, H. J.; Pack, J. D. *Phys. Rev. B* **1976**, *13*, 5188.
(46) Frisch, M. J.; *Gaussian 03, Revision C.02*; Gaussian, Inc.: Wallingford, CT, 2004.
(47) Leech, C. J.; Fabbiani, F. P. A.; Shankland, K.; David, W. I. F.; Ibberson, R. M. *Acta Crystallogr. B* **2008**, *64*, 101.

Table 1. Refined Unit Cell Parameters for SQBP Determined from Variable-Temperature X-ray Powder Diffraction Experiments[a]

	lattice parameters						
T/K	*a*/Å	*b*/Å	*c*/Å	*β*/°	volume/Å^3	R_{wp}^{Pawley}	data range/° 2*θ*
270	3.7900(1)	11.2073(1)	27.4336(1)	92.386(1)	1164.25(3)	18.36	2.5−36.0
293	3.7997(1)	11.2098(1)	27.4523(1)	92.223(1)	1168.42(3)	10.43	0.5−40.6
320	3.8097(1)	11.2133(1)	27.4704(1)	92.080(1)	1172.74(3)	17.85	2.5−36.0
370	3.8325(1)	11.2236(1)	27.5108(1)	91.749(1)	1182.82(3)	17.70	2.5−36.0
420	3.8539(1)	11.2347(1)	27.5398(2)	91.479(1)	1192.00(3)	8.19	3.0−40.0
	12.3463(3)	11.2960(1)	9.0503(1)	108.919(1)	1194.00(3)		
493	12.4624(3)	11.3141(1)	9.0940(1)	109.459(1)	1209.02(3)	13.84	0.5−35.5

[a] Note that the volume expansion of form-I in the range 270−420 K is essentially linear ($r^2 = 0.9991$ for a linear regression fit).

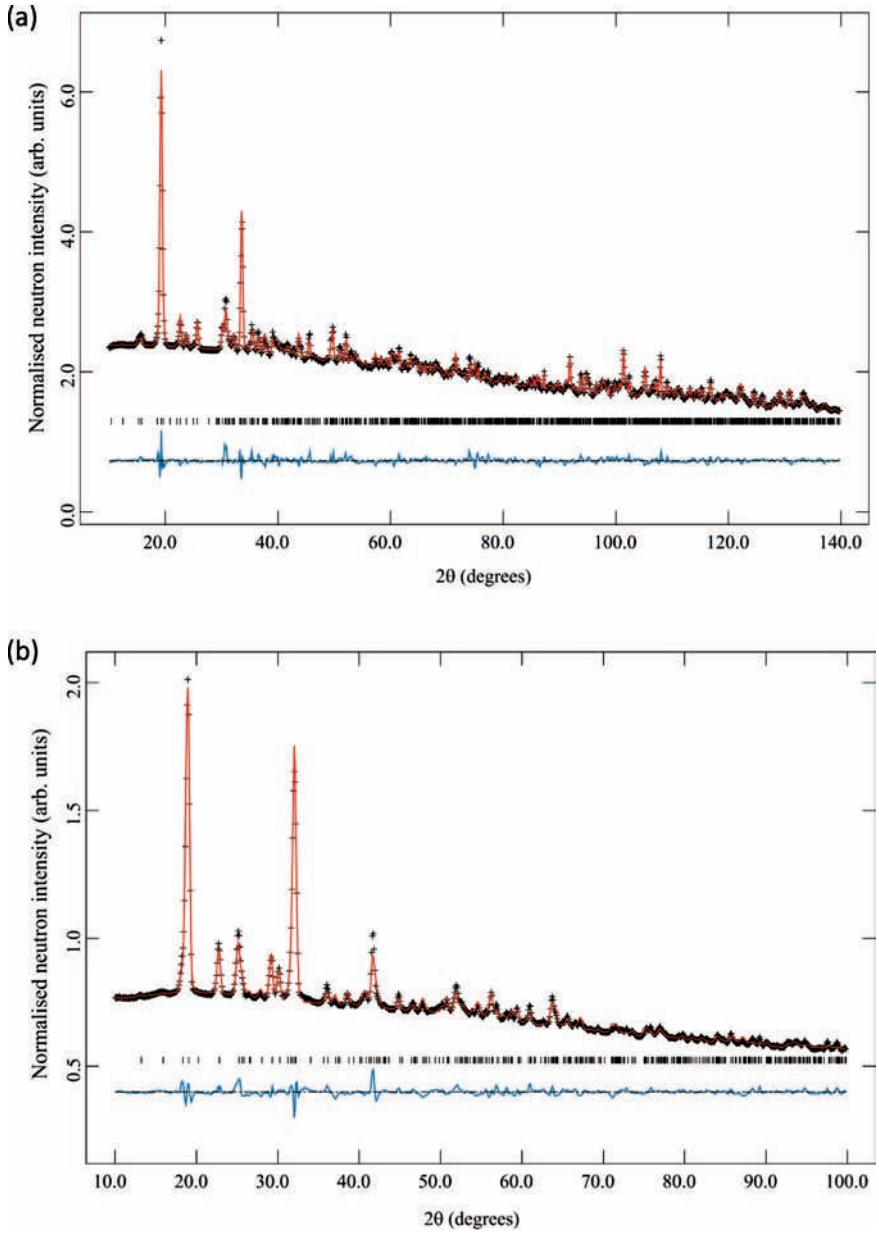

Figure 3. Rietveld refinements of the D20 neutron diffraction patterns of (a) SQBP form-I at 120 K and (b) SQBP form-II at 473 K. The crosses denote the observed diffraction profile; in (a) the solid line is the profile calculated using the 180 K single-crystal X-ray structure of form-I as the starting model, with coordinates refined under geometrical restraints. The line below the pattern shows the difference between the measured and the calculated patterns. The ticks indicate the positions of the Bragg peaks.

Institut Laue-Langevin, Grenoble, France. The very high incident flux of this instrument allowed data acquisition times of just 20 min for form-I and 60 min for form-II on a nondeuterated sample. Both structures were refined very satisfactorily (see Figure 3) using heavy-atom geometrical restraints (bond lengths, angles, and planarity) and thermal parameter constraints derived from the X-ray structures. Not only does this study confirm that the form-II structure is best described as $[BPH_2]^{2+}$ hydrogen-bonded to $[SQ]^{2-}$, but it also illustrates how powder neutron diffraction data collected at high intensity

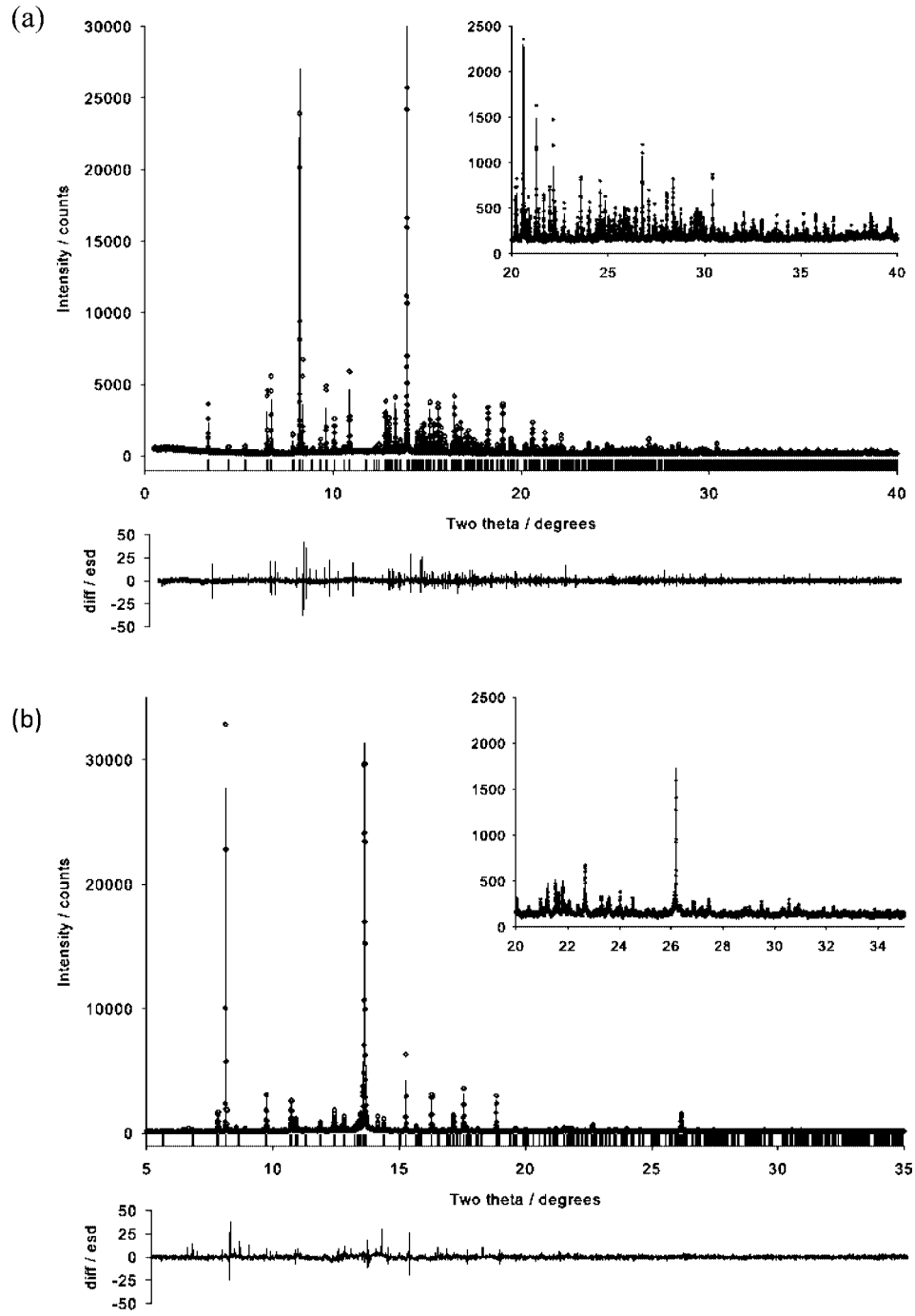

Figure 4. Pawley fit to the X-ray powder diffraction pattern of (a) SQBP form-I at 293 K and (b) SQBP form-II at 493 K. The circles denote the observed data; the line is the calculated profile. The line below the pattern shows the difference between the measured and the calculated patterns, expressed as $[(y_{obs} - y_{calc})/\sigma(y_{obs})]$. The ticks indicate the positions of the Bragg peaks; the refined lattice parameters and R_{wp} are listed in Table 1.

sources can be used to study nondeuterated organic compounds. Such a capability has important implications for the future study of molecular materials such as pharmaceuticals using neutron powder diffraction.[47]

3.4. Powder X-ray Diffraction. This study was undertaken to examine the reversibility of the form-I to form-II phase transition with temperature. The experiments were carried out using the high-resolution powder-diffraction beam line (ID31) located at the European Synchrotron Radiation Facility (ESRF), Grenoble. Pawley refinement using the 293 K data set gave a good fit to the data (see Figure 4a), with the refined lattice parameters presented in Table 1. This demonstrated that the measurement on the single crystal was representative of the bulk polycrystalline material. It should be noted, however, that three very weak reflections in the powder pattern (at $2\theta = 6.84°$, 8.54°, and 8.91°) were not accounted for in the Pawley refinement, indicating that the sample contained a very small amount of an unidentified impurity.

Pawley refinement using the 493 K data set gave a good fit to the data (see Figure 4b), with the refined lattice parameters presented in Table 1. The sample clearly contained an additional component (possibly residual form-I), but it was not possible to obtain a satisfactory indexing solution or Pawley refinement to identify this component unambiguously.

Table 2. Effective Mulliken charges, *q*(e), borne by BP and SQ Molecules, the Lower and Upper Edge Energies (eV), Widths (eV), and Assignments of the Topmost Valence and Lowermost Conduction Bands in Forms-I and -II of the SQBP Crystal

form	*q*(BP)	*q*(SQ)	band	E_{lower}	E_{upper}	E_{width}	assignment
I (LT)	+0.715	−0.715	valence	−5.589	−5.381	0.208	SQ C + O
			conduction	−2.477	−2.344	0.133	BIPY C + N
II (HT)	+1.297	−1.297	valence	−5.050	−4.880	0.170	SQ C + O
			conduction	−2.884	−2.666	0.218	BIPY C + N

The sample was subsequently cooled over a period of ∼10 h, over which time four further data sets were collected. The diffraction pattern obtained at 420 K (see Figure 5) could be satisfactorily fitted to a mixture of forms-I and -II, with the refined lattice parameters presented in Table 1. This confirms that, at least under these conditions, form-II reverts to form-I, not the additional polymorph as proposed by Reetz et al.[15] The diffraction patterns obtained during the remaining data collections of the cooling process all gave good fits consistent with the predominance of a single phase, namely form-I (see Table 1). This significant hysteresis shows clearly the existence of a kinetic barrier that must be overcome in order to convert form-II back to form-I. These results also explain the observations from the DSC experiments that showed that on first heating a sample of form-I an endotherm of 5.4 kJ mol^{-1} was measured, but in subsequent cooling and heating cycles energy changes of only 4.2 kJ mol^{-1} were measured. At the relatively rapid heating and cooling rates used in the DSC experiments, there was insufficient time for all of form-II to transform back to form-I on cooling, and hence, in subsequent heating and cooling cycles the energy changes were smaller.

We can conclude that all of the heating experiments show an abrupt change to given form-II. This is particularly noticeable in the powder XRD measurements where the transition temperature was very distinct, occurred over only a few degrees, and was complete. We therefore concur that the transition form-I to form-II is independent of the rate of heating. In contrast, on cooling the high-temperature form-II persisted for much longer

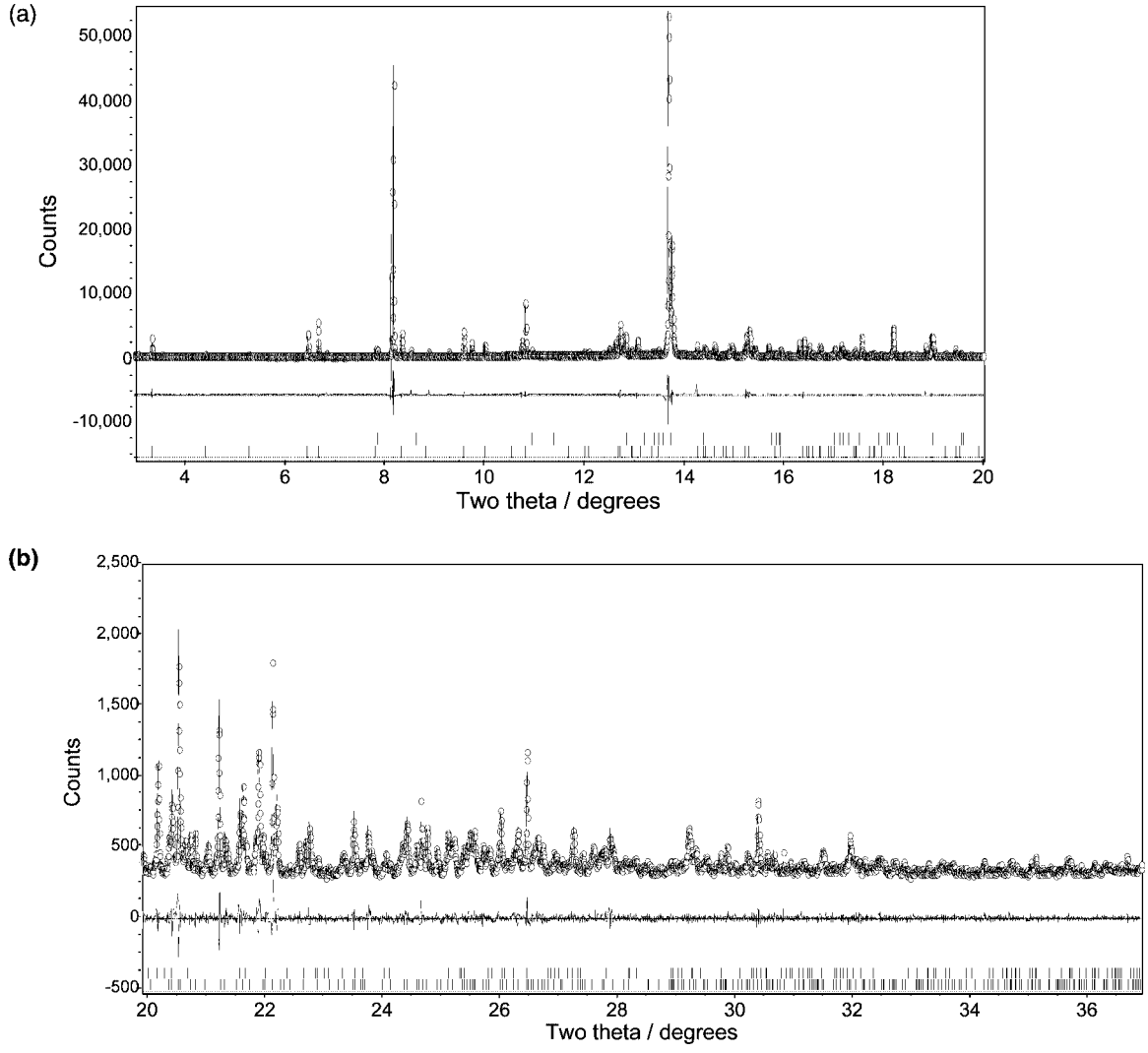

Figure 5. Two-phase Pawley fit to the X-ray powder diffraction pattern of a sample comprising SQBP forms-I and -II at 420 K, showing (a) low-angle and (b) high-angle regions. The circles denote the observed data; the line is the calculated profile. The line below the pattern shows the difference between the measured and the calculated patterns, expressed as $[(y_{obs} - y_{calc})]$. The ticks indicate the positions of the Bragg peaks in form-I (lower set of ticks) and form-II (upper set); the refined lattice parameters and R_{wp} are listed in Table 1.

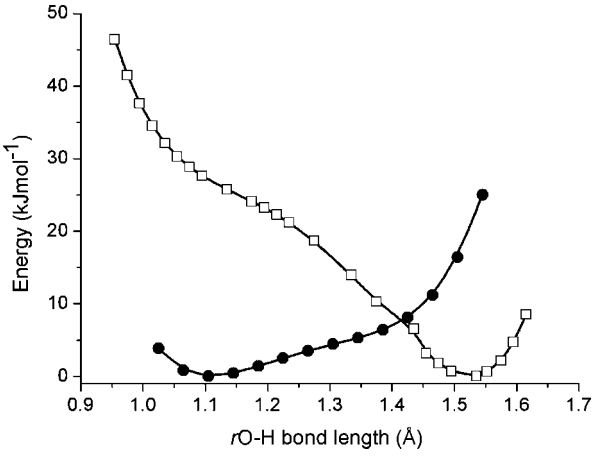

Figure 6. Calculated potential energy surfaces for the hydrogen-bond linkage present in form-I (filled circles) and form-II (open squares).

periods at temperatures well below the transition temperature. It is for this reason that we propose that there exists a kinetic barrier for interconversion from form-II to form-I.

3.5. Simulation. Selected parameters obtained in the PW-DFT geometry optimizations of both forms of SQBP can be found in Table 1 in the Supporting Information, together with the experimental data for direct comparison. The calculated parameters are generally in very good agreement with the X-ray data, yielding average deviations of around 1% and 2% in form-I and form-II, respectively. The agreement with the neutron data is also good, with average deviations observed of less than 3% for both phases.

The structure optimization of form-II was run in parallel with the neutron diffraction experiments, and therefore used the single-crystal X-ray diffraction lattice parameters and heavy atom coordinate set with ions present in their $[SQ]^{2-}$ and $[BPH_2]^{2+}$ forms as a starting point. The calculations revealed that this structure was indeed a stable point on the potential energy surface. Location of the correct proton positions in the hydrogen bonds was central to this study. The optimized geometries obtained for both forms were subsequently confirmed as the lowest points on their respective potential energy surfaces by performing series of single-point energy calculations in which a single hydrogen atom was incrementally displaced along the N···O hydrogen bond vector connecting SQ and BP molecules. Two separate sets of calculations were performed: first, a proton in the form-I structure was moved from a $[SQH]^-$ molecule to $[BPH]^+$, mimicking the form-I to form-II phase transition; while, in the second, a proton in the form-II structure was moved from $[BPH_2]^{2+}$ back to $[SQ]^{2-}$, thus mimicking the reverse phase transition. The energy profiles obtained from both sets of linear PES scans are plotted in Figure 6.

The potential energy surfaces reveal many important properties of the hydrogen-bond linkages. First, the minimum energy structures found in the geometry optimizations are clearly observed (yielding O−H distances around 1.1 and 1.5 Å, with the latter corresponding to an N−H bond length of 1.07 Å). For each form only one stable minimum exists, although a shoulder on each surface corresponding to the proton-transferred form is evident. The energy well corresponding to the form-I structure is shallower than that of form-II, where the proton appears to require less than 10 kJ mol^{-1} to adopt a conformation similar to that of form-II. For form-II the barrier to revert to a form-I-like structure is much higher (around 30 kJ mol^{-1}). This suggests that the hydrogen bond proton in form-I is more labile than that in form-II, which could in turn account for the observations from the DSC and powder diffraction reversibility studies that the form-II to form-I transition appears to be controlled by kinetic factors.

The dynamical stability of both forms was then explored within MD simulations, which revealed that both states of protonation are stable at finite temperature. Furthermore, the time-averaged model for form-II obtained from the MD (which was run in the absence of symmetry constraints) was consistent with the *C*2/*c* space group obtained from the X-ray diffraction experiments. To probe further the suggestion raised by the PES scans that the hydrogen bond protons in form-I are more labile than those in form-II, time-averaged O−H and N−H bond lengths were obtained from the MD simulations. The first 0.15 ps of the trajectories were discarded to allow for equilibration, the average O−H and N−H distances in form-I and form-II, respectively, were computed, and standard errors estimated by straightforward application of a blocking method.[48] Thus, the time-averaged O−H distance in form-I equates to 1.270(30) Å, as compared with 1.113(2) Å for the N−H distance in form-II. The larger value and significant uncertainty obtained for the former bond indicates that the dynamical simulations support the attributions of proton lability made on the basis of the static calculations.

We now turn to consider the relative stabilities of form-I and form-II, as well as the nature of the proton-transfer process that takes place during the phase transition. The plane-wave and localized basis set calculations concur that form-II possesses lower internal energy than form-I. However, the differences are very small, amounting to 6.2 and 4.4 kJ mol^{-1}, respectively, both of which lie well within the range expected for polymorphs of molecular compounds.[49] The isolated molecule calculations offer some useful insight into this process, revealing in particular that the reaction in which the remaining proton transfers from the $[SQH]^-$ anion to the $[BPH]^+$ cation is very strongly disfavored in the gas phase, with an associated energy difference of the order of 1100 kJ mol^{-1}. The fact that this process occurs at all in the solid state must be a direct consequence of the increased electrostatic stabilization arising from the change in the charge states of the molecular ions, as well as their arrangement within the lattice.

A semiquantitative treatment of these interactions can be obtained from the application of a model for a one-dimensional chain of ions of alternating sign. The energy per pair is given by

$$E = \frac{-2\ln(2)q^2}{4\pi\varepsilon_0 R}$$

where the factor 2 ln(2) is the Madelung constant for a 1D chain, q is the magnitude of the charges borne by the ions, and R is the separation of the ions. Figure 7 shows the energy difference obtained between the two charged states of the chains, $\Delta E = E(q_2) - E(q_1)$ for the 'ideal' case ($q_1 = \pm 1e$, $q_2 = \pm 2e$), as well as with the effective Mulliken charges of the molecules shown in Table 2 ($q_1 = \pm 0.715e$, $q_2 = \pm 1.297e$). It should be noted, however, that the latter values must be regarded as establishing only relative variations for the absolute values have little formal meaning and are strongly basis set dependent.[50] The electrostatic stabilization produced by use of the ideal

(48) Flyvbjerg, H.; Petersen, H. G. *J. Chem. Phys.* **1989**, *91*, 461.
(49) Chisholm, J. A.; Motherwell, S.; Tulip, P. R.; Parsons, S.; Clark, S. J. *Cryst. Growth Des.* **2005**, *5*, 1437.
(50) Wiberg, K. B.; Rablen, P. R. *J. Comput. Chem.* **1993**, *14*, 1504.

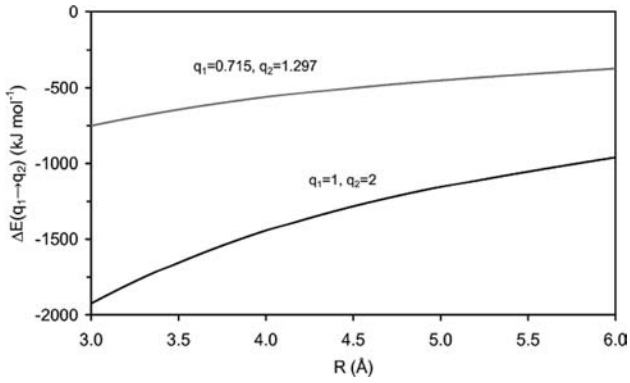

Figure 7. Difference in electrostatic energies per ion pair, ΔE (kJ mol^{-1}), between one-dimensional ionic chains with alternating charges of $\pm q_1$ and $\pm q_2$ as a function of ionic separation, R (Å).

charges more than offsets the large energy difference obtained from the isolated molecule calculation for separations of less than ca. 5.5 Å. However, the stabilizations arising from the use of the calculated charges are much smaller and are not sufficient to balance the energy deficit at any reasonable separation. This is likely due to an underestimate of the effective charges within the Mulliken analyses in which the net charge transfer between molecules in the conformations appropriate to form-I and form-II amounts to only 0.582e.

A more accurate treatment of the electrostatic interactions can be obtained by performing an Ewald sum[51] over the Mulliken charges of the individual atoms, yielding an energy difference between the two forms of 414.9 kJ mol^{-1}. This is within the range of stabilizations produced by the 1D chain model using the same charges and presumably represents an underestimate for essentially the same reasons. We anticipate that the charges obtained by application of a basis-independent method, such as a topological analysis or a calculation of the dynamical charge tensors, would offer further insights, but this lies outside the scope of the present work. The current results suffice to establish that the small energy difference separating the polymorphic forms in the solid state arises out of the counterbalancing of two much larger contributions.

It should be noted that the addition of the vibrational zero point energies to the internal energies of the isolated molecules destabilizes the high temperature structure by 4.5 kJ mol^{-1} relative to form-I. While this value has been obtained within a strictly harmonic analysis and does not include the red-shifts of the donor-proton stretching modes accompanying hydrogen bond formation, it does raise the issue that the relative free and internal energies of the two forms may differ substantially. Furthermore, it is conceivable that the inclusion of vibrational contributions may render form-I more stable than form-II, as expected on the basis of the DSC measurements. We conclude from this that future theoretical studies of both the current material, as well as of polymorphic molecular crystals in general, should include an explicit treatment of the thermodynamics obtained from the direct integration of the phonon dispersion relations across the Brillouin zone.

The atom-projected densities-of-states plots for both forms are shown in Figure 8, while Table 2 presents the relevant band edges, widths, and assignments. It is clear that both structures are wide gap charge-transfer insulators, in which the fundamental optical excitation corresponds to the transfer of an

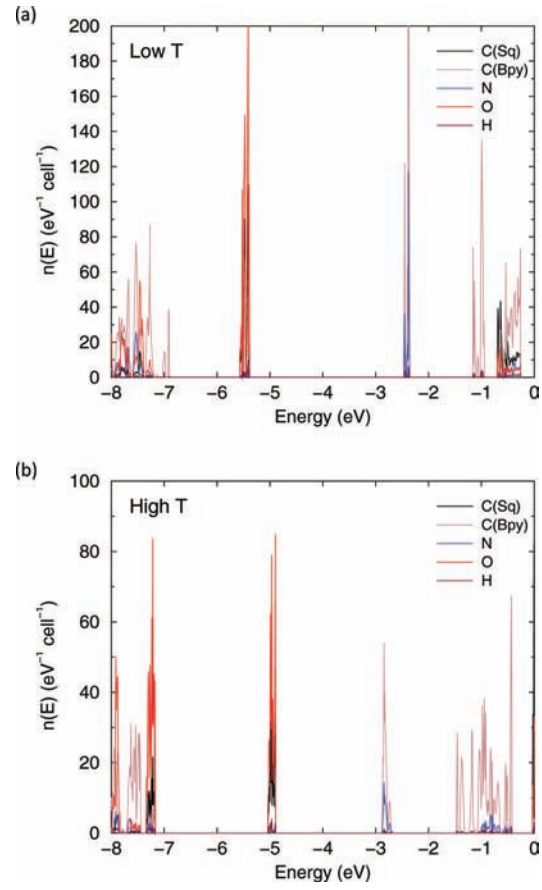

Figure 8. Atom-projected densities-of-states plot for (a) form-I and (b) form-II. The valence band edge lies at −5.38 and −4.88 eV for the two polymorphs, respectively.

electron from the SQ(C + O) π-states to the BP(C + N) π*-states. We note in particular that the BP-derived conduction bandwidth increases notably in the form-II lattice; this is likely due to the fact that the BP molecules are planar in this structure, leading to an enhanced overlap of the π* states resident on both rings.

There remains the question of why the phase transition leads to a change in color. In order to investigate whether there is a link between the changes in color and the protonation states of the molecules in the crystalline adducts, the values of the calculated band gaps were sought. Equating the optical absorption energy with the gap separating the peak densities in the uppermost valence and lowermost conduction bands yields theoretical values of 403 and 566 nm in form-I and form-II, respectively, in reasonable agreement with the experimental values of 450 and 540 nm, respectively.

A direct explanation for the color change emerges from the understanding that there are two opposing interactions underlying the band shifts. First, there is the change in the site-specific Madelung potential due to the increase in the charges borne by the SQ and BP ions within the extended lattice framework. This would work to stabilize the SQ-derived valence band due to the increased positive charge at neighboring BP ions and to destabilize the BP-derived conduction band for essentially the opposite reason. Second, we must consider the changes in intramolecular potential due to variations in screening and electron−electron repulsion arising due to the change in ionic charge, which would be expected to yield shifts in the opposite sense to those just discussed.

(51) Allen, M. P.; Tildesley, D. J., *Computer Simulation of Liquids*; Clarendon Press: Oxford, 1989.

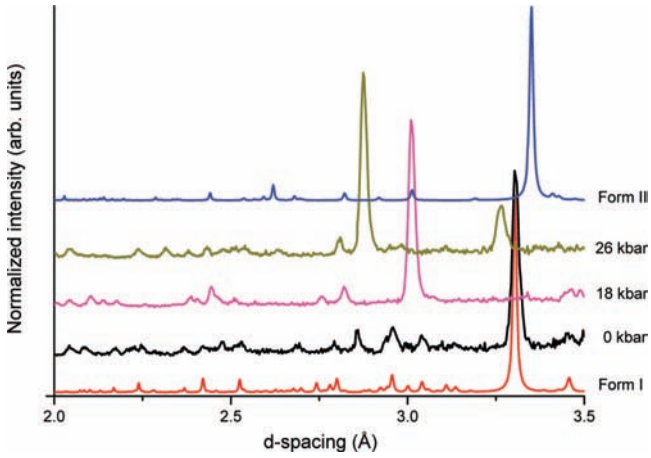

Figure 9. Comparison of the variable-temperature and variable-pressure powder diffraction patterns. Note the patterns shown for form-I (298 K) and II (453 K) were calculated using X-ray scattering factors, whereas the high-pressure patterns are derived from neutron measurements. Thus, while the peak intensities for the two different experiments are not comparable, the peak positions are as they dependent solely on unit-cell dimensions. Note also that the neutron diffraction patterns also contain peaks due to the pressure calibrant Pb.

The band shifts observed in our calculations suggest, therefore, that the intramolecular interactions dominate over the Madelung contributions. We note, for comparison, that progress from the singly to the doubly charged species in the isolated molecule calculations shifts the SQ HOMO upward by +5.3 eV, and the BP LUMO downward by −3.8 eV. The much smaller shifts of ∼ +0.5 and −0.4 eV, respectively, observed in the solid state make plain the extent to which the long-range electrostatic interactions suppress band motion.

3.6. Pressure. Finally, we report briefly on the experimental structural response of SQBP to pressure. The color change from yellow to red also occurred on increasing the pressure applied to a single crystal, but during this process the crystal was destroyed. Powder neutron diffraction experiments indicated that the sample underwent two phase transitions at 18 and 26 kbar but reverted back to form-I on decompression to ambient conditions (i.e., the transitions are completely reversible). The patterns obtained for these two high-pressure forms are clearly different from those of form-I and form-II (see Figure 9), casting doubt on Reetz's suggestion that the high-temperature and high-pressure forms are the same.[15] Nevertheless, it is very likely that all of the forms will have structural similarities, and the observed color change suggests that proton-transfer is once again involved. All attempts to index the powder patterns for the two high-pressure forms have, however, proven to be unsuccessful. This aspect of the work is therefore incomplete, and further work will be required to confirm the proton-transfer nature of the pressure-induced phase transition.

4. Conclusions

Using a combination of experimental techniques, this work has shown that the 1:1 adduct formed between squaric acid and 4,4′-bipyridine undergoes a temperature-induced first-order phase transition to form a structure containing the doubly protonated bipyridine ion and the squarate dianion. On cooling, this high-temperature form-II exhibits significant hysteresis, resulting in the formation of a mixture of both forms-I and II, thereby indicating the presence of a kinetic barrier for conversion of form-II to form-I. Evidence for the presence of two further phases at high pressure has also been obtained.

Computational modeling studies indicate that forms-I and -II are stable, low-energy structures. For each polymorph only one proton position on the hydrogen-bond potential energy surface is observed. The proton associated with the hydrogen bond in form-I appears to be more labile than that of form-II, which may account for the kinetic barrier associated with the II → I transition on cooling. The yellow-to-red color change associated with the I → II transition is due to the narrowing of the SQ → BP charge-transfer energy gap evident from comparisons of the densities-of-states plots of both forms. We attribute the narrowing to the fact that while the proton-transfer induced variations in the Madelung potential and intramolecular interactions are of comparable magnitude, they do not cancel completely, so that the domination of the latter effects destabilize the valence bands derived from the squaric acid molecule and stabilize the conduction bands derived from the bipyridine molecule.

Acknowledgement. We thank the EPSRC for funding under Grants No. GR/T21615 and GR/T21608 (C.C.W., C.A.M.) and also under EP/E051049 and EP/050859 (M.T.W., C.C.W.). C.A.M. also acknowledges the Royal Society for the award of a University Research Fellowship. This work has made use of the resources provided by the EaStCHEM Research Computing Facility (http://www.eastchem.ac.uk/rcf). This facility is partially supported by the eDIKT initiative (http://www.edikt.org). We thank the STFC (formerly CCLRC), ESRF, and ILL for allocation of beamtime.

Supporting Information Available: Table of selected geometric parameters from experiment and theory for SQBP forms-I and -II; CIF files from the diffraction analyses; optical and infrared spectra; complete ref 46. This material is available free of charge via the Internet at http://pubs.acs.org.

JA8082973